Proc. Natl. Acad. Sci. USA
Vol. 95, pp. 8026–8033, July 1998
Biophysics

This contribution is part of the special series of Inaugural Articles by members of the National Academy of Sciences elected on April 29, 1997.

Inhibitor binding changes domain mobility in the iron–sulfur protein of the mitochondrial *bc*1 complex from bovine heart

HOEON KIM*†, DI XIA*†, CHANG-AN YU‡, JIA-ZHI XIA‡, ANATOLY M. KACHURIN‡, LI ZHANG‡, LINDA YU‡, AND JOHANN DEISENHOFER*§

*Howard Hughes Medical Institute and Department of Biochemistry, University of Texas Southwestern Medical Center, Dallas, TX 75235-9050; and ‡Department of Biochemistry and Molecular Biology, Oklahoma State University, Stillwater, OK 74078-0454

Contributed by Johann Deisenhofer, May 18, 1998

ABSTRACT **We have analyzed crystal structures of cytochrome *bc*1 complexes with electron transfer inhibitors bound to the ubiquinone binding pockets Q_i and/or Q_o in the cytochrome *b* subunit. The presence or absence of the Q_i inhibitor antimycin A did not affect the binding of the Q_o inhibitors. Different subtypes of Q_o inhibitors had dramatically different effects on the mobility of the extramembrane domain of the iron–sulfur protein (ISP): Binding of 5-undecyl-6-hydroxy-4,7-dioxobenzothiazol and stigmatellin (subtype Q_o–II and Q_o–III, respectively) led to a fixation of the ISP domain on the surface of cytochrome *b*, whereas binding of myxothiazol and methoxyacrylate-stilbene (subtype Q_o–I) favored release of this domain. The native structure has an empty Q_o pocket and is intermediate between these extremes. On the basis of these observations we propose a model of quinone oxidation in the *bc*1 complex, which incorporates fixed and loose states of the ISP as features important for electron transfer and, possibly, also proton transport.**

Ubiquinol–cytochrome-*c* oxidoreductase (cytochrome *bc*1 complex; EC 1.10.2.2) is a segment of the respiratory chain in mitochondria and of the photosynthetic apparatus of purple bacteria. It catalyzes electron transfer (ET) from ubiquinol to cytochrome *c*, coupled to proton transport across a membrane (from the matrix space to the intermembrane space of mitochondria; from the cytoplasm to the periplasm of purple bacteria). The resulting electrochemical proton gradient drives ATP synthesis and transport processes (1, 2). Essential for the function of the *bc*1 complex are the three redox proteins cytochrome *b*, cytochrome *c*1, and the iron–sulfur protein (ISP). Two *b*-type hemes (b_L and b_H) are attached to cytochrome *b*, one c-type heme is bound to cytochrome *c*1, and a Rieske-type iron–sulfur center (FeS) is bound to ISP (2). Whereas some bacterial *bc*1 complexes consist of only those redox subunits (3), their mitochondrial counterparts contain up to 8 additional protein subunits whose precise functions in the complex are largely unknown (4).

The protonmotive Q cycle model (2, 5, 6) best explains experimental results on the ET pathway through the four redox centers of the *bc*1 complex. It postulates two separate ubiquinone binding sites, called Q_o and Q_i. In *bc*1 complexes of the inner membrane of mitochondria, Q_o is located near the membrane surface facing the intermembrane space, and Q_i is near the membrane surface facing the matrix space. The Q cycle model requires bifurcated electron flow from ubiquinol bound in the Q_o site: The first electron of ubiquinol is sequentially transferred to the ISP, cytochrome *c*1, and eventually to the soluble cytochrome *c*. Protons are released into the intermembrane space, generating a ubisemiquinone anion in the Q_o site. The second electron is transferred to hemes b_L and b_H and to a ubiquinone or a ubisemiquinone anion in the Q_i site. The fully reduced quinone in the Q_i site picks up two protons from the matrix space and moves to the Q_o site for recycling.

The discovery of different types of specific ET inhibitors of the *bc*1 complex was crucial for the development of this Q cycle hypothesis. The two major types of *bc*1 inhibitors are called Q_o or Q_i inhibitors, depending on their action in the cytochrome *bc*1 complex (7, 8). All Q_i inhibitors target specifically the ET path from heme b_L to ubiquinone/ubisemiquinone in the Q_i site; they do not share common structural motifs. Q_o inhibitors block binding of quinol to the Q_o site and ET through this site. They can be classified further on the basis of common structural motifs and of their effects on the absorption spectrum of heme b_L and on the electron paramagnetic resonance (EPR) spectrum and redox potential of the FeS (7). One Q_o inhibitor subtype shares a methoxyacrylate (MOA) group (examples: myxothiazol, MOA-stilbene), another subtype resembles a hydroxyquinone molecule (example: 5-undecyl-6-hydroxy-4,7-dioxobenzothiazol or UHDBT), and a third subtype has a chromone group as the common motif (example: stigmatellin). MOA inhibitors cause solely a red-shift of the b_L heme's spectrum (9) and hydroxyquinone inhibitors alter the EPR spectrum of the FeS (10), whereas the chromone inhibitors affect both spectra (11).

The possibility of two inhibitor binding sites in the Q_o pocket has led to the so-called "catalytic switch" model (12). This model assumed at least two conformational states of the Q_o pocket in cytochrome *b*, which are directly controlled by the redox state of the ISP. By alternating between these two conformational states, bifurcated ET is enforced during the catalytic reaction. Separately, the "double Q_o occupancy" model was recently proposed; it is based on the observation of two distinct EPR signals that depend on the redox state or on ubiquinone concentration in bacterial *bc*1 complexes. According to this model, the Q_o pocket has two ubiquinone binding sites with different affinities (13, 14). Later, this became one of the foundations of the "proton-gated charge-transfer" model that integrates ET and proton translocation (15).

Abbreviations: ET, electron transfer; ISP, iron–sulfur protein; FeS, iron–sulfur center; MOA, methoxyacrylate; UHDBT, 5-undecyl-6-hydroxy-4,7-dioxobenzothiazol.

†H.K. and D.X. contributed equally to this work.

§To whom reprint requests should be addressed at: HHMI and Department of Biochemistry, UT Southwestern Medical Center, 5323 Harry Hines Blvd., Dallas, TX 75235-9050. e-mail: Johann.Deisenhofer@email.swmed.edu.

Recently, the crystal structure of the bovine *bc*1 complex was reported, and the binding sites of the Q_i inhibitor antimycin A and of the Q_o inhibitor myxothiazol were identified (16). The two binding sites are formed by the cytochrome *b* subunit near opposite membrane surfaces. They are close to iron positions determined from anomalous scattering data. Here, we report further crystallographic studies of inhibitor binding to the *bc*1 complex and studies of the effects of different types of inhibitors on the ISP and the location of its FeS.

MATERIALS AND METHODS

Protein Preparation. Cytochrome *bc*1 complex from bovine heart mitochondria was prepared, starting from highly purified succinate–cytochrome-*c* reductase (17) as described previously (16, 18). *bc*1 particles were solubilized by deoxycholate, and contaminants were removed by a 15-step ammonium acetate fractionation. Pure *bc*1 complex in the oxidized form was recovered from the precipitates formed between 18.5% and 33.5% saturation with ammonium acetate. For crystallization, this material was adjusted to a final concentration of 20 mg/ml in a solution containing 50 mM Mops buffer at pH 7.2, 20 mM ammonium acetate, 20% (wt/vol) glycerol, and 0.1% either decanoyl-*N*-methylglucamide or diheptanoyl phosphatidylcholine.

Cocrystallization with Inhibitors. For cocrystallization of the *bc*1 complex with various inhibitors, a 2-fold molar excess of inhibitors was added to the protein solution. This solution was set up for crystallization as described (16, 18). Crystals grew in 3–4 weeks; they had a rectangular shape and ranged in size from 0.4 mm to 0.7 mm. They could be frozen at high glycerol concentration, and they had the same symmetry (space group $I4_122$) and similar unit cell dimensions as the native crystals: $a = b = 153.5$ Å, $c = 597.7$ Å.

Data Collection and Analysis. When flash frozen and kept at 100 K, the crystals were stable enough in strong x-ray beams to allow collection of complete sets of diffraction data. Data were collected on imaging plates at beamlines X4A, X12B, and X25 of the National Synchrotron Light Source (NSLS) at Brookhaven National Laboratory, beamline BL4 of the European Synchrotron Radiation Facility (ESRF), and at beamline 7-1 of Stanford Synchrotron Radiation Laboratory (SSRL). The raw diffraction data were processed with the DENZO/HKL package (19); Bijvoet pairs were kept separated. Programs MTZUTILS, SCALEIT, and FFT from the CCP4 package (20) were used for merging and scaling the data with the native data and for the calculation of difference-Fourier maps. Phases for the structure factors of inhibitor-bound crystals in the resolution range 20–3.0 Å were calculated, starting from the native multiple isomorphous replacement phase set (20- to 3.5-Å resolution), by density modification and phase extension in small steps [program DM (21)]. The position and orientation of the extramembrane domain of the ISP were determined by searching electron density maps (20- to 3.0-Å resolution), using the high-resolution structure of this domain (22) as a search model. The search procedure (D.X. *et al*., unpublished work) calculated linear correlation coefficients between map density and model density under variation of the model orientation or position. First, the FeS of the model was translated to the experimentally determined cluster position in the crystal and the model was systematically rotated around this position. The orientation of maximal correlation was further refined by alternating scans of small shift and orientation ranges until convergence was reached.

RESULTS

Fig. 1 shows an overall view of our current model of the dimeric *bc*1 complex. Crystallographic refinement of this model is in progress and will be reported elsewhere; the model includes 15,600 non-hydrogen atoms; the values of R_{work} and R_{free} in the resolution range of 20–2.7 Å are 0.313 and 0.378, respectively. Phases calculated from this model without the ISP extramembrane domain were used in our real-space searches for the orientation of this domain.

We cocrystallized the bovine *bc*1 complex with the Q_i inhibitor antimycin A and with the Q_o inhibitors myxothiazol, MOA-stilbene, UHDBT, and stigmatellin, and with combinations of antimycin A and each of the Q_o inhibitors. The crystallization behavior of the *bc*1 complex mixed with inhibitors was similar to that of the native protein (18); the cocrystals were isomorphous with the native crystals, and the x-ray diffraction data obtained from these crystals were of comparable quality. Table 1 lists statistics up to 3.0-Å resolution of the diffraction data sets used in this study; some of the data sets, including Native 1, extend well beyond that resolution. Using multiple isomorphous replacement phases improved by solvent flattening (16), we analyzed each cocrystal by calculating difference-density maps (structure factor amplitudes: $|F_I| - |F_N|$, where $|F_I|$ and $|F_N|$ are amplitudes of inhibitor-containing crystals and native crystals, respectively) and anomalous difference maps (structure factor amplitudes: $|F^+| - |F^-|$, where $|F^+|$ and $|F^-|$ are amplitudes of Bijvoet pairs of reflections from the same crystal). In all cases, the difference-density maps clearly showed electron density for the inhibitors (Fig. 2). Binding of the Q_o inhibitors was independent of the presence or absence of the Q_i inhibitor, and *vice versa*. This result was expected because of the spatial separation of the binding sites near opposite membrane surfaces (16), and it is consistent with the experimental observation of additive inhibitory activity of these two major inhibitor types.

Antimycin A. The difference-density maps contained strong positive density for antimycin A itself near heme b_H (Figs. 2*A* and 5). Except for local changes near the antimycin A binding site, the maps did not indicate any antimycin A-induced change elsewhere in the *bc*1 structure. In particular, the presence of antimycin A did not influence the positions and relative heights of the peaks representing the iron centers in the anomalous difference maps (Table 2). Strong negative density appeared next to the positive density for antimycin A; its elongated shape resembled that of a ubiquinone molecule (Fig. 2*B*). Difference-density maps between native crystals soaked with either ubiquinone-10 or ubiquinone-6, and native crystal, had their highest peaks at this site (data not shown). We assume that a ubiquinone molecule was bound in the native structure but displaced by antimycin A; this assumption is consistent with spectroscopic observations (23). It appears that the Q_i binding site is not identical to the antimycin A binding site, but close enough for overlap, with antimycin A reaching deeper into the binding pocket.

Q_o Site Inhibitors. The Q_o inhibitors occupy different subsites in the Q_o pocket. Except for the combination MOA-stilbene/UHDBT, their binding sites overlap, which explains why binding of these Q_o inhibitors is mutually exclusive (24, 25). Myxothiazol and MOA-stilbene bind close to the heme b_L, UHDBT binds close to the FeS, and stigmatellin overlaps both binding sites (Figs. 2*F* and 5). This finding is in perfect agreement with the aforementioned spectroscopic changes caused by binding of these inhibitors to the *bc*1 complex. Different binding regions for different Q_o inhibitors were also predicted from functional studies on inhibitor-resistant mutants (26–29). On the basis of these observations, the Q_o inhibitors used in this study can be divided into three categories: Q_o-I (myxothiazol, MOA-stilbene), Q_o-II (UHDBT), and Q_o-III (stigmatellin) (7).

Binding of Q_o inhibitors had considerable influence on the heights and positions of peaks corresponding to the FeS in the anomalous difference maps. More importantly, there was a strong correlation between the change in this anomalous signal

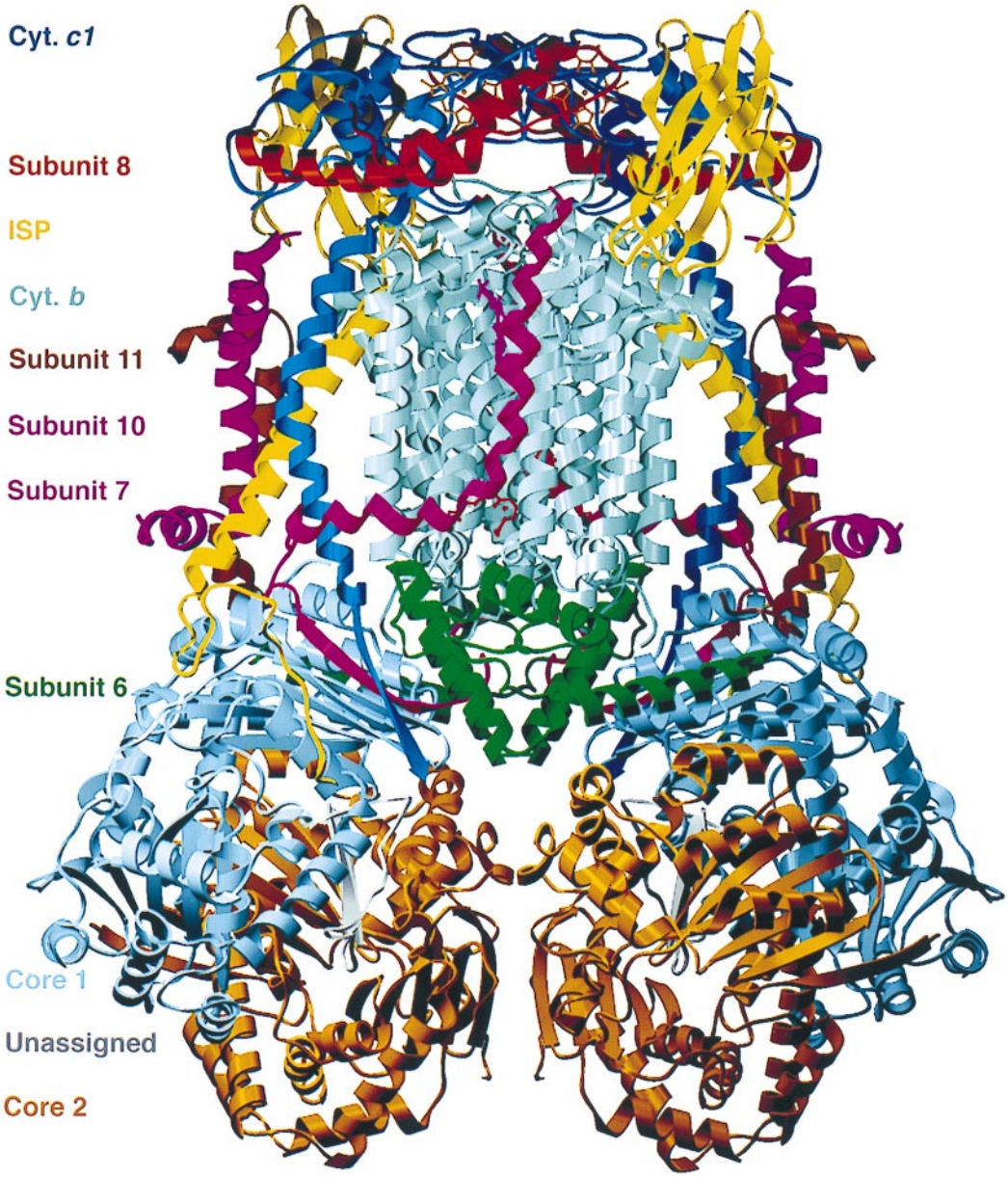

FIG. 1. Ribbon model of the dimeric cytochrome *bc*1 complex. Colors identifying the subunits are given at the left margin. An as-yet-unassigned peptide is bound in a cavity formed by subunits core 1 and core 2 (16). Figs. 1 and 5 were prepared with the programs MOLSCRIPT (33) and SETOR (34), respectively.

(compared with that of native crystals) and the subtype of the Q_o inhibitor. Binding of MOA-stilbene (type Q_o-I) abolished the anomalous signal for the FeS at the position observed in the native crystals (Table 2). Instead, a minor peak appeared closer to cytochrome *c*1, 15 Å away from the native position (Fig. 3*A*). Although small compared with the other peaks, it

Table 1. X-ray diffraction data statistics ($d_{min} \geq 3.0$ Å)

Data set	λ, Å	d_{min}, Å	Unique reflections	Observations	Mean redundancy	Completeness, %	Mosaicity, °	$I/\sigma(I)$	R_{merge}, %
Native 1*	1.01	3.0	65,901	1,715,432	26.0	91.6	0.620	16.2	14.0
Native 2†	1.74	3.2	43,969	601,180	13.7	74.7	0.555	12.7	9.8
Antimycin A‡	1.55	3.4	45,286	586,286	12.9	89.9	0.602	14.9	10.7
MOA-stilbene§	0.99	3.0	63,789	1,054,638	16.5	89.9	0.750	19.0	4.9
UHDBT¶	1.08	3.0	68,766	1,382,177	20.1	96.8	0.727	12.0	11.2
Stigmatellin§	0.99	3.0	50,387	736,039	14.6	68.8	0.678	6.2	19.6
Antimycin A + MOA-stilbene†	1.74	3.3	56,192	809,082	14.4	92.5	0.394	15.4	11.0
Antimycin A + myxothiazol†	1.74	3.0	65,729	940,740	14.3	92.2	0.474	7.6	14.7
Antimycin A + UHDBT†	1.74	3.5	45,755	808,324	17.7	96.6	0.628	11.8	13.1
Antimycin A + stigmatellin¶	1.08	3.3	51,414	554,575	10.8	94.8	0.564	16.0	7.4

X-ray data were collected from the beamlines X25(*), X12B(‡), and X4A(†) of the Brookhaven National Laboratory, BL4 (§) of the European Synchrotron Radiation Facility, and 7-1(¶) of the Stanford Synchrotron Radiation Laboratory.

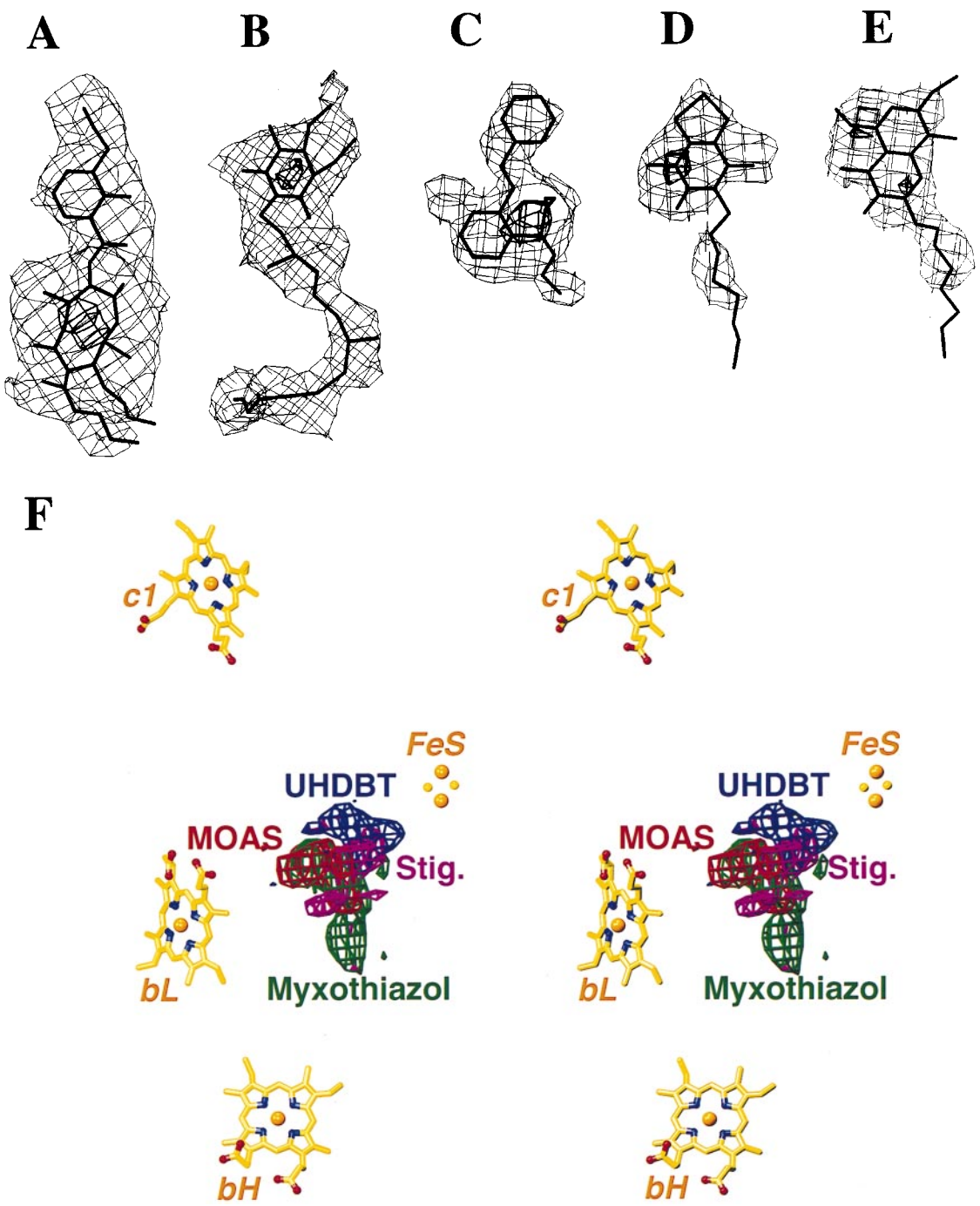

FIG. 2. (*A–E*) Difference electron densities between the inhibitor-bound and native crystals and atomic models of inhibitors and ubiquinone. The maps are contoured at two levels (thin and thick lines, respectively); contour levels for each map are listed in standard deviations from the mean. (*A*) Antimycin A (3, 20). (*B*) Ubiquinone (−3, −10). (*C*) MOA-stilbene (3, 8). (*D*) UHDBT (3, 7). (*E*) Stigmatellin (3, 5). (*F*) Stereo drawing: Models of redox cofactors together with superimposed difference-densities of four Q_o inhibitors, viewed parallel to the membrane. MOAS, MOA-stilbene; Stig., stigmatellin.

appeared consistently in all forms of MOA-stilbene-containing crystals (Table 2), and it may represent a weakly occupied alternative position of the FeS. Most likely, the changes in the FeS signal indicate increased mobility of the extramembrane domain of the ISP (22), which, because of its rigidity, would be able to perform a hinged motion relative to its transmembrane domain. Positive and negative difference-density between native crystals and the inhibitor cocrystals, spread over the entire ISP region, indicated a conformational change of the whole extramembrane domain of the ISP (data not shown). The absence of difference-density in the transmembrane region of the ISP showed that the ISP subunit was not accidentally lost from the complex.

Myxothiazol, which belongs to the same Q_o-I subtype as MOA-stilbene, causes a significant lowering, but not the disappearance, of the anomalous signal for the FeS (Table 2). If the strength of this signal is a measure of the mobility of the ISP extramembrane domain, the effects of MOA-stilbene and myxothiazol on this mobility go in the same direction, with MOA-stilbene being the more potent of the two.

In contrast to the Q_o-I inhibitors, UHDBT (type Q_o-II) caused an increase of the anomalous signal of the FeS (Table 2 and Fig. 3*C*) and strong positive density for the ISP, for example, in the difference-density map between the UHDBT-bound and the native structures (Fig. 4). This density covered

Table 2. Peaks in anomalous difference maps

Data set	Maximum peak height, units of σ	Normalized peak height*				
		b_H	b_L	$c1$	FeS†	Next-highest peak
Native 1	14.7	1.00	0.99	0.53	0.45	0.28
Native 2	27.6	1.00	0.93	0.61	0.47	0.18
Antimycin A	14.3	1.00	1.09	0.78	0.60	0.40
MOA-stilbene	14.2	1.00	1.02	0.76	—	0.53‡
UHDBT	13.3	1.00	0.89	0.61	0.97	0.34
Stigmatellin	18.8	1.00	0.99	0.79	1.18	0.28
Antimycin A + MOA-stilbene	29.2	1.00	0.96	0.57	—	0.20‡
Antimycin A + myxothiazol	20.1	1.00	0.97	0.66	0.38	0.24
Antimycin A + UHDBT	21.8	1.00	0.77	0.60	0.83	0.32
Antimycin A + stigmatellin	13.3	1.00	0.95	0.56	1.25	0.36

*Normalization to b_H peak.
†FeS position in the fixed state.
‡Possible alternative position of FeS in the loose state.

a region of the right shape and volume to fit the entire extramembrane domain of the ISP, indicating that the whole domain underwent a transition to a less mobile or completely immobilized state, in which it is bound to the surface of cytochrome *b*.

Binding of stigmatellin (type Q_o-III) had an immobilizing effect on the ISP domain similar to that caused by UHDBT. Stigmatellin, which binds more strongly than UHDBT to most *bc*1 complexes (30), caused a larger increase in the height of the anomalous peak for the FeS than did UHDBT (Table 2).

ISP Extramembrane Domain. In the crystal structure of native *bc*1 complex, the parts protruding into the intermembrane space were represented by weak, uninterpretable electron density (16). We used the position of the FeS obtained from anomalous scattering maps and the high-resolution model of the extramembrane domain of the ISP (22) in a rigid body search in real space to determine the orientation of the ISP domain. For this purpose we calculated electron density maps with data from crystals of native *bc*1 complex and of cocrystals with inhibitors. We used model phases to 3-Å resolution after cyclic solvent flattening; the starting phases did not contain contributions from the ISP extramembrane domain, and the solvent mask excluded an appropriate region around the iron position from flattening. Table 3 summarizes the results of our rigid body searches. Clearly, the orientation of the ISP domain was defined best for complexes containing the inhibitors of types Q_o-II and Q_o-III, with the correlation for stigmatellin slightly higher than for UHDBT. Fig. 5 shows the ISP domain in the orientation with optimal correlation; it contacts the extramembrane surface of cytochrome *b*. The correlation was significantly weaker in the native structure and very weak for myxothiazol and MOA-stilbene. A search around the possible alternative iron position in MOA-stilbene gave a very weak correlation, demonstrating that the structure of the ISP domain is not well defined in these crystals. The results of these searches support our interpretation that the decrease in the heights of the anomalous FeS peaks indicates a decreasing occupancy of the ISP domain bound to the surface of cytochrome *b*, with the occupancy strongest in the presence of stigmatellin and weakest in the presence of MOA-stilbene.

DISCUSSION

We have shown that different types of inhibitors of quinol oxidation by the cytochrome *bc*1 complex prefer different subsites within the Q_o binding site in the cytochrome *b* subunit. This preference correlates well with the known spectroscopic effects of the Q_o inhibitors on heme b_L and/or on the FeS; it is not affected by the presence or absence of the Q_i inhibitor antimycin A. Binding of Q_o inhibitors has a dramatic effect on the conformational state of the ISP's extramembrane domain: synonymous changes in the relative heights of FeS peaks in anomalous difference maps and in the correlations of a model density of the extramembrane ISP domain with unbiased electron densities in the various cocrystals indicate a large change in mobility of this domain. The *bc*1 crystals used in our studies are particularly suitable for observing such changes because the protein domains located in the mitochondrial intermembrane space–i.e., the extramembrane parts of cytochrome *c*1 and the ISP, and subunit 8—do not participate in crystal contacts, and can therefore undergo free movements or conformational transitions.

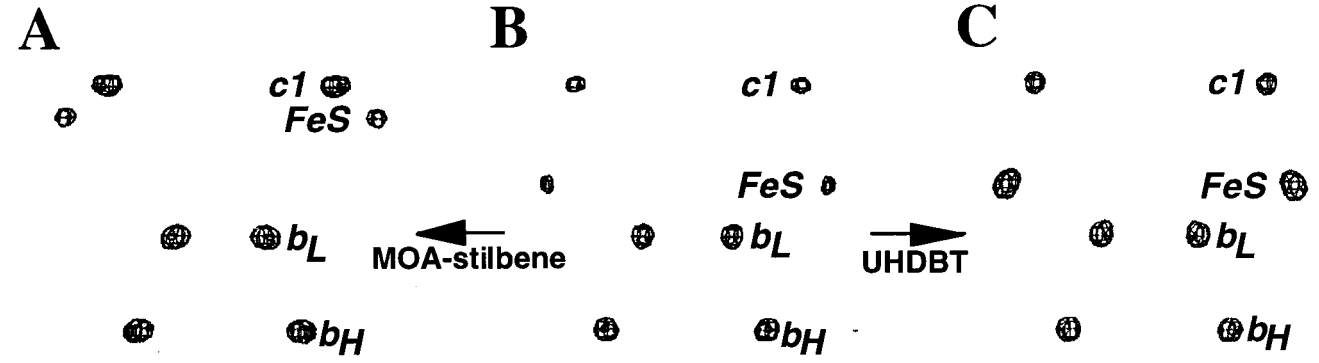

FIG. 3. Anomalous difference maps at 5-Å resolution of crystals containing MOA-stilbene (*A*), no inhibitor (native) (*B*), and UHDBT (*C*); the four redox centers are labeled. The maps are contoured at five standard deviations above the mean. The peak for the FeS in the UHDBT is stronger than the one in the native structure but becomes equivalent in the UHDBT-bound structure (Table 2).

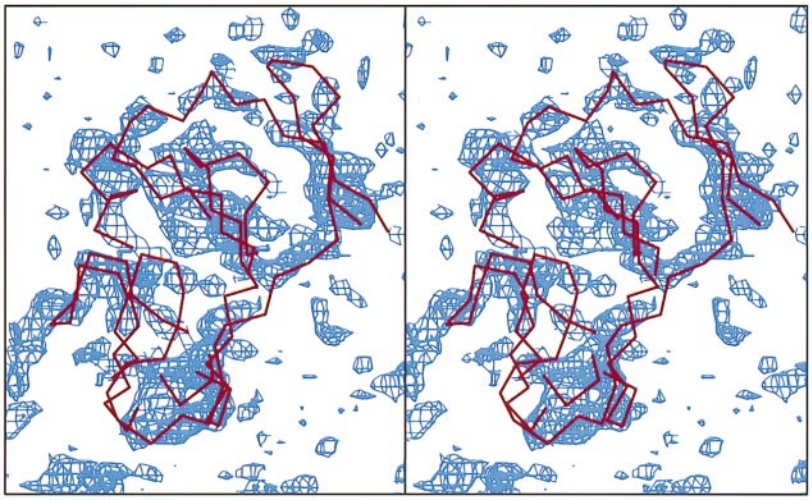

FIG. 4. Stereo drawing: Difference-density map (blue) between the UHDBT-bound and native structures, contoured at the 2-σ level. Overlaid is the C^{α} trace (red) of the extramembrane domain of the ISP (22).

In crystals of native *bc*1 (Q_o binding pocket empty), the ISP extramembrane domains appear to be partitioned between a fixed state and a loose state. Only the molecules in the fixed state can be observed by crystallography; they are bound to the surface of cytochrome *b*, above the surface helices cd1 and cd2 (Fig. 5). The FeS in the fixed state is 31 Å away from the iron in cytochrome *c*1; this distance makes fast ET between the FeS and the *c*1 heme unlikely.

Binding of myxothiazol or MOA-stilbene [type Q_o-I (7)] shifts the equilibrium toward the loose state, as indicated by decreased anomalous FeS peak heights and density correlations. MOA-stilbene binding even leads to the complete disappearance of fixed ISP molecules and to the appearance of a new peak in the anomalous difference map, 15 Å away from the native position. This peak and a weak density correlation could indicate an alternative conformation of the ISP, in which the ISP would make close contact with cytochrome *c*1, rotated by 134° relative to the native orientation. However, because of the weakness of the density correlation and of the iron signal from anomalous scattering, we have to assume that this state, if it exists, is very poorly populated.

In contrast, the binding of UHDBT (type Q_o-II) and stigmatellin (type Q_o-III) strongly increases the population of the fixed ISP state. These inhibitors, although making intimate contacts with cytochrome *b*, also directly contact the ISP near the FeS. A close contact between stigmatellin and FeS was expected because of the large increase of the FeS's redox potential upon inhibitor binding (11, 25). The detailed molecular mechanism of the transition of the ISP extramembrane domain from a fixed to a loose state in response to binding of ligands in the Q_o site must await the completion of crystallographic refinement of the atomic model and the collection of crystallographic data on quinone binding at the Q_o site.

One of the most important features of the Q cycle hypothesis is the bifurcation of ET at the Q_o site, the mechanism of which is still under investigation. The transition between a fixed and a loose state of the ISP extramembrane domain can be integrated into a functional model of quinol oxidation very similar to the catalytic switch model proposed by Brandt and von Jagow (12). This model proposes that, upon reduction of FeS, the Q_o center switches from an "FeS-state" that allows ET from the Q_o site only to FeS, to a "b-state" that allows ET only to heme b_L. The "b-state" in this model corresponds well to the loose state, whereas the "FeS-state" resembles the fixed state.

To combine our observations with the catalytic switch model, we assume two transient quinone binding sites in the inhibitor binding pocket. One of these putative sites, designated P1, is closer to ISP where UHDBT binds; the other site, designated P2, is closer to b_L heme where MOA-stilbene binds. Analogous to inhibitor binding, binding of quinol to P1 will cause the fixation of ISP, and binding of semiquinone to P2 will release the ISP from this fixed state. With these assumptions, the ET events at the Q_o site can be described as follows: A cycle starts with ubiquinol bound to P1, and the oxidized ISP in the fixed state. The first electron is transferred from ubiquinol to the FeS; the two protons are released. The ubisemiquinone moves to P2, causing a conformational transition in which the ISP is in the loose state. The reduced ISP in the loose state approaches cytochrome *c*1 and may form a transient complex with it; this allows rapid ET from the FeS to the *c*1 heme. The second electron is transferred from ubisemiquinone in P2 to heme b_L, and subsequently to b_H and to ubiquinone or ubisemiquinone in the Q_i site. The ubiquinone in P2 dissociates from the *bc*1 complex to be replaced by another ubiquinol molecule, which will occupy P1 and bring the ISP back to the fixed conformational state.

Table 3. Constrained real space rotational and translational search with an extramembrane fragment of ISP as a search model

Maps used in searches	Angular rotation,* °	Changes in distance relative to native, Å	Maximum c.c. (×1000)	σ above mean, *n*	Second-largest c.c. (×1000)	σ above mean, *n*
Native	0.0	0.0	186.6	11.4	68.1	4.1
UHDBT	3.3	0.7	313.1	15.5	84.9	3.8
Stigmatallin	4.2	1.1	309.8	17.6	76.3	3.9
Myxothiazol	10.6	1.2	102.1	5.9	67.7	3.9
MOAS†	134.2	15.1	73.1	4.7	61.6	3.9

c.c., Linear correlation coefficient.
*Angular rotation is defined as a rotation that brings the position of ISP in inhibitor bound forms to the native position.
†Putative new position of ISP in MOA-stilbene-bound *bc*1 crystal.

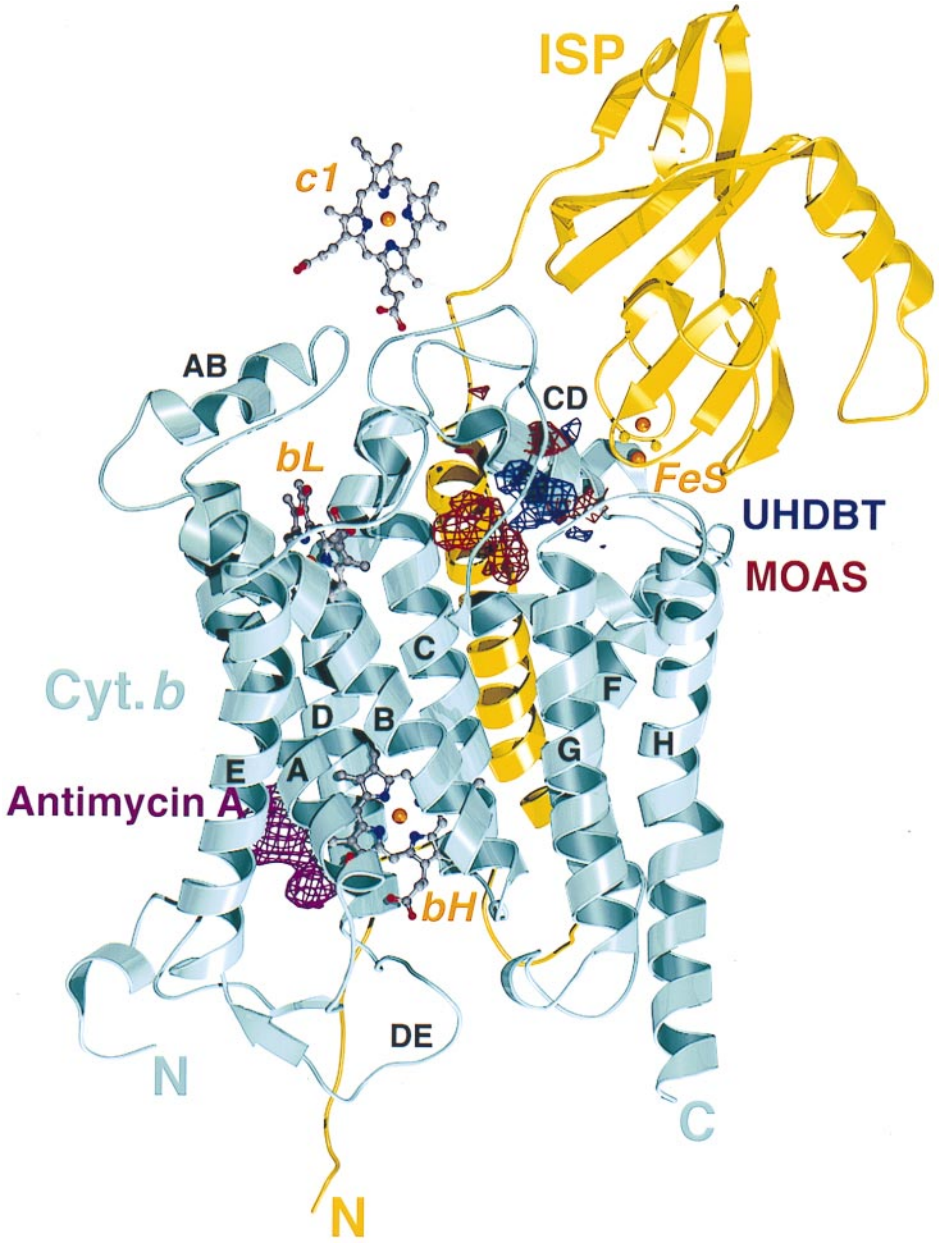

FIG. 5. Cytochrome *b* and ISP, hemes, and difference densities for MOA-stilbene (MOAS), UHDBT, and antimycin A, viewed parallel to the membrane. The eight transmembrane helices of cytochrome *b* are labeled A to H; some of the connecting loops are labeled too. The loop CD consists of two antiparallel helices. The structure of the extramembrane domain of ISP is based on the crystal structure of this domain (22), positioned and oriented by using UHDBT data (Tables 1–3); the transmembrane helix of ISP contacts cytochrome *b* of the second monomer in the dimer (not shown).

One problem with this model is that especially Q_o-I inhibitors are chemically dissimilar to quinones, so that it is not clear whether ubisemiquinone binds in P2, and, if it does, whether it can cause the same structural changes as MOA-stilbene. Another problem is the lack of a detectable ubisemiquinone radical at the Q_o site. The reported detection of a transient, antimycin A-insensitive, ubisemiquinone radical at the Q_o site (31) was recently questioned (P. R. Rich, personal communication), as it was not sensitive to the Q_o site inhibitors such as myxothiazol, MOA-stilbene, or stigmatellin. An alternative hypothesis for the ET event at the Q_o site could avoid this difficulty by assuming that the two electrons of ubiquinol in the complex are transferred simultaneously, one to FeS, and the second to heme b_L and further to heme b_H; thus, no ubisemiquinone would be generated. In this scenario, movement of the quinone between Q_o subsites would probably not occur, and the conformational change of the cytochrome *b* protein, which switches the reduced ISP from the fixed to the loose state, would have a different cause. An attractive candidate for the switching event would be the ET from heme b_L to heme b_H; this mechanism would make sure that the second electron of ubiquinol would reach its destination before or at the same time as the first electron reaches heme *c*1. Thus, because the oxidation of the reduced FeS would depend on the transfer of an electron from heme b_L to heme b_H, bifurcation would be obligatory for the oxidation of ubiquinol in the *bc*1 complex.

During the preparation of this manuscript, Zhang *et al.* (32) reported the x-ray structure analysis of cytochrome *bc*1 complexes from chicken, beef, and rabbit; the four crystal forms described by these authors are all different from the one used in our work. One of the main findings was variability in the orientation of the extramembrane domain of the ISP in different crystal forms. In the presence of stigmatellin, the FeS

position in the chicken *bc*1 complex appears identical to the one in the fixed state reported here. In the absence of stigmatellin, the FeS was found closer to the cytochrome *c*1 heme, with the ISP domain apparently in alternative fixed states. At least in some of the crystal forms the ISP in these states seems to be involved in, and stabilized by, crystal contacts (32); this would also explain the higher crystalline order of cytochrome *c*1 and subunit 8 ("hinge") in these crystals. Nevertheless, the conclusion of Zhang *et al.* that the ISP extramembrane domain of the *bc*1 complex is mobile, and that its mobility has functional implications for ET, is identical to the conclusion we reached on the basis of our results.

We thank Dr. Stephen R. Sprang for thoughtful comments on the manuscript, Ms. Dorothee B. Staber for help with the manuscript, and the staff at beamlines X4A, X12B, and X25 at the National Synchrotron Light Source, BL-4 at the European Synchrotron Radiation Facility, and 7-1 at the Stanford Synchrotron Radiation Laboratory for help with data collection. This work was supported by National Institutes of Health Grant GM 30721 to C.-A.Y. and by a grant from the Welch foundation to J.D. J.D. is an Investigator in the Howard Hughes Medical Institute.

1. Trumpower, B. L. & Gennis, R. B. (1994) *Annu. Rev. Biochem.* **63,** 675–716.
2. Brandt, U. & Trumpower, B. L. (1994) *CRC Crit. Rev. Biochem. Mol. Biol.* **29,** 165–197.
3. Trumpower, B. L. (1990) *Microbiol. Rev.* **54,** 101–129.
4. Hatefi, Y. (1985) *Annu. Rev. Biochem.* **54,** 1015–1069.
5. Mitchell, P. (1976) *J. Theor. Biol.* **62,** 327–367.
6. Trumpower, B. L. (1990) *J. Biol. Chem.* **265,** 11409–11412.
7. von Jagow, G. & Link, T. A. (1986) *Methods Enzymol.* **126,** 253–271.
8. Link, T. A., Haase, U., Brandt, U. & von Jagow, G. (1993) *J. Bioenerg. Biomembr.* **25,** 221–232.
9. Brandt, U., Schägger, H. & von Jagow, G. (1988) *Eur. J. Biochem.* **173,** 499–506.
10. Bowyer, J. R., Edwards, C. A., Ohnishi, T. & Trumpower, B. L. (1982) *J. Biol. Chem.* **257,** 8321–8330.
11. Ohnishi, T., Brandt, U. & von Jagow, G. (1988) *Eur. J. Biochem.* **176,** 385–389.
12. Brandt, U. & von Jagow, G. (1991) *Eur. J. Biochem.* **195,** 163–170.
13. Ding, H., Robertson, D. E., Daldal, F. & Dutton, P. L. (1992) *Biochemistry* **31,** 3144–3158.
14. Ding, H., Moser, C. C., Robertson, D. E., Tokito, M. K., Daldal, F. & Dutton, P. L. (1995) *Biochemistry* **34,** 15979–15996.
15. Brandt, U. (1996) *Biochim. Biophys. Acta* **1275,** 41–46.
16. Xia, D., Yu, C.-A., Kim, H., Xia, J. Z., Kachurin, A. M., Zhang, L., Yu, L. & Deisenhofer, J. (1997) *Science* **277,** 60–66.
17. Yu, C.-A. & Yu, L. (1980) *Biochim. Biophys. Acta* **591,** 409–420.
18. Yu, C.-A., Xia, J.-Z., Kachurin, A. M., Yu, L., Xia, D., Kim, H. & Deisenhofer, J. (1996) *Biochim. Biophys. Acta* **1275,** 47–53.
19. Otwinowski, Z. & Minor, W. (1997) *Methods Enzymol.* **276,** 307–326.
20. Collaborative Computing Project No. 4 (1979) *A Suite of Programs for Protein Crystallography* (Daresbury Laboratory, Warrington, U.K.).
21. Cowtan, K. D. & Main, P. (1996) *Acta Crystallogr. D* **52,** 43–48.
22. Iwata, S., Saynovits, M., Link, T. A. & Michel, H. (1996) *Structure* **4,** 567–579.
23. Ohnishi, T. & Trumpower, B. L. (1980) *J. Biol. Chem.* **255,** 3278–3284.
24. von Jagow, G., Ljungdahl, P. O., Graf, P., Ohnishi, T. & Trumpower, B. L. (1984) *J. Biol. Chem.* **259,** 6318–6326.
25. von Jagow, G. & Ohnishi, T. (1985) *FEBS Lett.* **185,** 311–315.
26. Geier, B. M., Schägger, H., Brandt, U., Colson, A.-M. & von Jagow, G. (1992) *Eur. J. Biochem.* **208,** 375–380.
27. Robertson, D. E., Daldal, F. & Dutton, P. L. (1990) *Biochemistry* **29,** 11249–11260.
28. Tron, T., Crimi, M., Colson, A.-M. & Degli Esposti, M. (1991) *Eur. J. Biochem.* **199,** 753–760.
29. Tron, T. & Lemesle-Meunier, D. (1990) *Curr. Genet.* **18,** 413–419.
30. Geier, B. M., Haase, U. & von Jagow, G. (1994) *Biochem. Soc. Trans.* **22,** 203–209.
31. de Vries, S., Albracht, S. P. J, Berden, J. A. & Slater, E. C. (1982) *Biochim. Biophys. Acta* **681,** 41–53.
32. Zhang, Z. L., Huang, L. S., Shulmeister, V. M., Chi, Y. I., Kim, K. K., Hung, L. W., Crofts, A. R., Berry, E. A. & Kim, S. H. (1998) *Nature (London)* **392,** 677–684.
33. Kraulis, P. J. (1991) *J. Appl. Crystallogr.* **24,** 946–950.
34. Evans, S. V. (1993) *J. Mol. Graph.* **11,** 134–138.